研究成果の刊行に関する一覧表

雑誌

発表者氏名	論文タイトル名	発表誌名	巻号	ページ	出版年
Irie T, Matsuzaki Y, Sekino Y, Hirai H	Kv3.3 channels harbouring a mutation of spinocerebellar ataxia type 13 alter excitability and induce cell death in cultured cerebellar Purkinje cells.	The Journal of Physiology.	592 (Pt 1)	229-247	2014
Usami M, Mitsunaga K, Irie T, Miyajima A, Doi, O.	Proteomic analysis of ethanol-induced embryotoxicity in cultured post-implantation rat embryos.	The Journal of Toxicological Sciences.	39	285-292	2014
Usami M, Mitsunaga K, Irie T, Nakajima M.	Various definitions of reproductive indices: a proposal for combined use of brief definitions.	Congenital Anomalies.	54(1)	67-68	2014
Usami M, Mitsunaga K, Irie T, Miyajima A, Doi O	Simple in vitro migration assay for neural crest cells and the opposite effects of all-trans-retinoic acid on cephalic- and trunk-derived cells.	Congenital Anomalies.	54(3)	184-188	2014

JPn Neuroscience
The Journal of Physiology
J Physiol 592.1 (2014) pp 229–247

Kv3.3 channels harbouring a mutation of spinocerebellar ataxia type 13 alter excitability and induce cell death in cultured cerebellar Purkinje cells

Tomohiko Irie[1,2], Yasunori Matsuzaki[2], Yuko Sekino[1] and Hirokazu Hirai[2]

[1]*Division of Pharmacology, National Institute of Health Sciences, Setagaya 158-8501, Japan*
[2]*Department of Neurophysiology, Gunma University Graduate School of Medicine, Maebashi, Gunma, 371-8511, Japan*

Key points

- The cerebellum plays crucial roles in controlling sensorimotor functions, and patients with spinocerebellar ataxia type 13 exhibit cerebellar atrophy and cerebellar symptoms.
- The disease is an autosomal dominant disorder caused by missense mutations in the voltage-gated K^+ channel Kv3.3, which is expressed intensely in the cerebellar Purkinje cells, the sole output neurons from the cerebellar cortex.
- Here, we examined how these mutations cause the cerebellar disease by lentiviral expression of the mutant Kv3.3 in mouse cultured Purkinje cells.
- Expression of the mutant Kv3.3 suppressed outward currents, broadened action potentials and elevated basal intracellular calcium concentration in Purkinje cells. Moreover, the mutant-expressing Purkinje cells showed impaired dendrites and extensive cell death, both of which were significantly rescued by blockade of P/Q-type Ca^{2+} channels.
- These results suggest that Purkinje cells in the patients also exhibit similar abnormalities, which may account for the pathology of the disease.

Abstract The cerebellum plays crucial roles in controlling sensorimotor functions. The neural output from the cerebellar cortex is transmitted solely by Purkinje cells (PCs), whose impairment causes cerebellar ataxia. Spinocerebellar ataxia type 13 (SCA13) is an autosomal dominant disease, and SCA13 patients exhibit cerebellar atrophy and cerebellar symptoms. Recent studies have shown that missense mutations in the voltage-gated K^+ channel Kv3.3 are responsible for SCA13. In the rodent brain, Kv3.3 mRNAs are expressed most strongly in PCs, suggesting that the mutations severely affect PCs in SCA13 patients. Nevertheless, how these mutations affect the function of Kv3.3 in PCs and, consequently, the morphology and neuronal excitability of PCs remains unclear. To address these questions, we used lentiviral vectors to express mutant mouse Kv3.3 (mKv3.3) channels harbouring an R424H missense mutation, which corresponds to the R423H mutation in the Kv3.3 channels of SCA13 patients, in mouse cerebellar cultures. The R424H mutant-expressing PCs showed decreased outward current density, broadened action potentials and elevated basal $[Ca^{2+}]_i$ compared with PCs expressing wild-type mKv3.3 subunits or those expressing green fluorescent protein alone. Moreover, expression of R424H mutant subunits induced impaired dendrite development and cell death selectively in PCs, both of which were rescued by blocking P/Q-type Ca^{2+} channels in the culture conditions. We therefore concluded that expression of R424H mutant subunits in PCs markedly affects the function of endogenous Kv3 channels, neuronal excitability and, eventually, basal $[Ca^{2+}]_i$, leading to cell death. These

DOI: 10.1113/jphysiol.2013.264309

results suggest that PCs in SCA13 patients also exhibit similar defects in PC excitability and induced cell death, which may explain the pathology of SCA13.

(Received 28 August 2013; accepted after revision 5 November 2013; first published online 11 November 2013)
Corresponding authors T. Irie: Division of Pharmacology, National Institute of Health Sciences, 1-18-1 Kamiyoga, Setagaya-ku, Tokyo 158-8501, Japan. Email: irie@nihs.go.jp or H. Hirai: Department of Neurophysiology, Gunma University Graduate School of Medicine, 3-39-22 Shouwa-machi, Maebashi-shi, Gunma 371-8511, Japan. Email: hirai@gunma-u.ac.jp

Abbreviations ACSF, artificial cerebrospinal fluid; AF, AlexaFluor; a.u., arbitrary unit; calbindin, calbindin D-28k; DIV, days *in vitro*; DNQX, 6,7-dinitroquinoxaline-2,3-dione; *G*, conductance; GFP, green fluorescent protein; hKv3.3, human Kv3.3; I_{Na}, Na^+ current; *k*, a slope factor; mKv3.3, mouse Kv3.3; MSCV, murine embryonic stem cell virus; PBS-XCG, PBS containing 0.3% Triton X-100, 0.12% λ-carrageenan, 1% goat serum and 0.02% sodium azide; PCs, Purkinje cells; P2A, 2A peptide sequence from porcine teschovirus-1; R_{max}, maximal fluorescence ratio; R_{min}, minimal fluorescence ratio; RT, room temperature; SCA13, spinocerebellar ataxia type 13; sEPSCs, spontaneous excitatory postsynaptic currents; τ_{acti}, activation time constant; τ_{inacti}, inactivation time constant; τ_{recove}, recovery time constant; VSV-G, vesicular stomatitis virus G protein; WT, wild-type.

Introduction

In most excitable cells, the high K^+ permeability arises from delayed-rectifier K^+ channels of the Kv class (Hille, 2001). One of the Kv subfamilies, known as Kv3, has generated particular interest because of its unique electrophysiological properties (Rudy & McBain, 2001). The Kv3 channels are high-voltage-activated K^+ channels, and they exhibit fast activation and deactivation kinetics; therefore, Kv3 channels are activated during action potential depolarization and are indispensable for high-frequency firing in many neurons, such as fast-spiking cortical interneurons and cerebellar Purkinje cells (PCs; Erisir *et al.* 1999; McKay & Turner, 2004). Rodents and humans possess four Kv3 genes: *Kv3.1–3.4*. The Kv3 channels are composed of four pore-forming subunits and form heterotetrameric channels by combination of Kv3 members. In the rodent brain, Kv3.3 mRNA and protein are abundantly expressed in the cerebellum, in which the mRNA is most intensely expressed in PCs (Weiser *et al.* 1994; Chang *et al.* 2007). Interestingly, Kv3.3-deficient mice show normal PC morphology and no ataxic phenotype (Joho *et al.* 2006; Hurlock *et al.* 2008; Zagha *et al.* 2010).

The numerous diseases arising from channel dysfunction (channelopathies) illustrate the importance of ion channels to the organism. To date, missense mutations in more than 60 ion-channel genes have been associated with human disease (Ashcroft, 2006). Recently, missense mutations in the *KV3.3* gene (also known as *KCNC3*), which encodes human Kv3.3 (hKv3.3) channels, were linked to autosomal dominant spinocerebellar ataxia type 13 (SCA13). Spinocerebellar ataxia type 13 is accompanied by cerebellar symptoms and by cerebellar atrophy, and three different mutations (R420H, R423H and F448L) have been identified, although the neurodegenerative changes in the post-mortem cerebellum have not been investigated (Waters *et al.* 2006; Figueroa *et al.* 2010). In *Xenopus* oocyte expression systems, coexpression of the R420H or R423H mutant subunits with wild-type (WT) hKv3.3 suppresses the current by a dominant-negative mechanism. Given the intense Kv3.3 expression in rodent PCs and the cerebellar atrophy in SCA13 patients, these mutations are expected to affect the neuronal excitability and morphology of PCs severely. Recently, Issa *et al.* reported that zebrafish expressing mutant zebrafish Kv3.3 subunits (homologous to the F448L mutant) in spinal motoneurons, which endogenously express Kv3.3, show defective axonal pathfinding (Issa *et al.*, 2012). However, as they used a motoneuron-specific enhancer to drive expression, these zebrafish display no distinct cerebellar abnormality. Therefore, the pathology of SCA13 has not been elucidated, and other methodological approaches are needed.

In the present study, to investigate the effects of *Kv3.3* mutations in PCs, we expressed mouse Kv3.3 (mKv3.3) channels harbouring the R424H missense mutation, which corresponds to the R423H mutation in hKv3.3, using a lentivirus system in mouse cerebellar cultures. Immunohistochemical analysis revealed that expression of R424H mutant subunits induced impaired dendrite development and cell death in PCs by 11 days *in vitro* (DIV) without significant alteration in granule cells. To examine the effects of R424H mutant subunits on the electrophysiological properties and free $[Ca^{2+}]_i$ of PCs, we performed whole-cell patch-clamp recordings and calcium imaging from PCs at DIV 8–10. Action potential duration and basal $[Ca^{2+}]_i$ were significantly increased in R424H mutant-expressing PCs compared with PCs expressing WT mKv3.3 or those expressing green fluoresent protein (GFP) alone. Furthermore, blockade of P/Q-type Ca^{2+} channels by ω-agatoxin IVA in the culture conditions rescued the dendritic maldevelopment and cell death in PCs caused by R424H mutant subunits.

Methods

Ethical approval

Newborn (i.e. within 24 h after birth) mice (ICR strain) of both sexes were used for cerebellar cultures. *Xenopus* oocytes were collected from anaesthetized *Xenopus laevis*. These animals were used according to the Guiding Principles for the Care and Use of Laboratory Animals approved by the guidelines of the National Institute of Health Sciences, Japan. All experiments also complied with *The Journal of Physiology* policy and UK regulations on animal studies (Drummond, 2009).

Molecular biology

The mouse cerebellum expresses the *Kv3.3b* gene, which is an alternatively spliced isoform of *mKv3.3* (Goldman-Wohl *et al.* 1994). *mKv3.3* cDNA that is nearly identical to *Kv3.3b* (Desai *et al.* 2008) was obtained as a kind gift from Dr Leonard K. Kaczmarek (Yale University, New Haven, CT, USA). The amino acid identity between hKv3.3 (Gene Accession number: AF055989) and mKv3.3 is 89%, and the sequence of the S4 transmembrane segment showed a complete match between the two species (Supplemental Fig. S1). To date, several reports have shown that there are three types of missense mutations (R420H, R423H and F448L) in hKv3.3 channels in distinct SCA13 pedigrees (Waters *et al.* 2006; Figueroa *et al.* 2010, 2011). In the present study, we focused on the R423H mutation. The S4 transmembrane segment of mKv3.3 has an arginine residue at position 424, which corresponds to the arginine at position 423 in hKv3.3. The arginine of mKv3.3 was replaced with histidine by overlap PCR using PrimeSTAR HS DNA Polymerase (Takara Bio, Shiga, Japan). The nucleotide exchanges were c.1271G>A and c.1272T>C. Wild-type and R424H mutant *mKv3.3* cDNA were subcloned in pcDNA3 (Invitrogen, Carlsbad, CA, USA), and the mutation was confirmed by sequencing.

For lentiviral vector-based gene expression, the murine embryonic stem cell virus (MSCV) promoter, which drives PC-predominant expression of a transgene in cerebellum, was used (Hawley *et al.* 1994; Hanawa *et al.* 2004; Torashima *et al.* 2006; Takayama *et al.* 2008). A Kozak translation initiation sequence and 2A peptide sequence from porcine teschovirus-1 (P2A) for efficient cleavage of polyproteins were placed at the N- and C-termini of WT and R424H mutant *mKv3.3* cDNA, respectively (Szymczak *et al.* 2004; Torashima *et al.* 2009). Then, stop codons were removed using the following PCR primer pair: a 5′ primer with an *Age*I site and Kozak sequence (bold; 5′ primer, CGACCGGT**GCCACC**ATGCT CAGTTCAGTGTGCGT) and a 3′ primer with an *Age*I site and P2A (bold; 3′ primer, CGACCGGT**GGCCCGG GTTTTCTTCAACATCTCCTGCTTGCTTTAACAGAG AGAAGTTCGTGGC**GCCGGAGCCGAGGATGGAGGG CAGGGTCG). A Gly-Ser-Gly linker (underlined in the 3′ primer) was also placed between the N-terminus of a WT (or R424H mutant) mKv3.3 sequence and P2A using the 3′ primer. This linker improves the cleavage efficacy of the P2A (Szymczak *et al.* 2004). The PCR products were subcloned in-frame into the *Age*I site of pCL20c MSCV-GFP, which is present 8 bp upstream from the translation initiation site of GFP. Finally, lentiviral transfer vectors for the experiments (pCL20c MSCV-WT-P2A-GFP and pCL20c MSCV-R424H-P2A-GFP) were obtained, and the inserted sequences were verified by sequencing.

Lentiviral vector preparation

Vesicular stomatitis virus G protein (VSV-G) pseudotyped lentiviral vector particles were produced by transient transfection of HEK 293T cells with viral plasmids as described previously (Torashima *et al.* 2006). In brief, HEK 293T cells were transfected with a mixture of the following four plasmids: pCAGkGP1R, pCAG4RTR2, pCAG-VSV-G and the lentiviral transfer vector plasmid (pCL20c MSCV-GFP, pCL20c MSCV-WT-P2A-GFP or pCL20c MSCV-R424H-P2A-GFP). The medium containing viral particles was concentrated by ultracentrifugation and resuspended in 70 μl of Dulbecco's phosphate-buffered saline (Wako Pure Chemical Industries, Osaka, Japan). The infectious titres of the virus were determined as follows: virus stocks were added to HEK 293T cells in the presence of Polybrene (6 μg ml^{-1}; Sigma-Aldrich, St Louis, MO, USA). After 4 days, GFP-positive cells were counted using a Tali Image-Based Cytometer (Invitrogen), and the titres were adjusted to 1.0×10^{10} or 0.5×10^{10} transduction units/ml.

Cerebellar culture and lentivirus-mediated gene expression

Cerebellar cultures were prepared according to our previous protocol with some modifications (Hirai & Launey, 2000). After the mice were killed by decapitation, the cerebella of newborn mice were quickly removed and treated with 2 ml of a papain digestion solution containing 40 units of papain (Worthington Biochemical, Lakewood, NJ, USA), 2 mM L-cysteine hydrochloride and 1 mM EDTA in Ca^{2+}–Mg^{2+}-free Hank's balanced salt solution (pH 7.0; Gibco, Grand Island, NY, USA; Tabata *et al.* 2000). Then, the cerebella were dissociated by trituration in Hank's balanced salt solution containing 0.05% (w/v) DNase (Sigma-Aldrich) and 12 mM $MgSO_4$. After centrifugation (180 × *g*, 5 min), the cells were resuspended in DMEM/F12 (Gibco)-based medium containing 4.2 mM

KCl, 1% (v/v) horse serum, 2% (v/v) B-27 (Gibco) and a mixture of a penicillin–streptomycin solution (1000 U ml^{-1} and 100 mg ml^{-1}, respectively; Gibco) to a density of 10×10^6 cells ml^{-1} (Gimenez-Cassina *et al.* 2007). High (25 mM)-KCl-containing medium, which is often used for rat cerebellar cultures, was not used in this study because low (5 mM)-KCl-containing medium can improve the long-term viability of mouse cerebellar granule cells, and high-KCl medium maintains the gene expression patterns of granule cells in an immature condition (Mellor *et al.* 1998; Sato *et al.* 2005). A mixture of the cell suspension (20 μl) and the concentrated virus solution (1 μl) was plated onto plastic coverslips (Cell Desk LF1, Sumilon MS-92132; Sumitomo Bakelite, Tokyo, Japan) coated with poly-D-lysine (Sigma-Aldrich) and incubated for 10 h in a CO_2 incubator for virus infection. The DMEM/F12-based medium (700 μl) was added to each dish and replaced by half once a week. Green fluorescent protein fluorescence was first observed at DIV 3, and its expression continued thereafter. In some experiments, ω-agatoxin IVA (0.2 μM; Peptide Institute, Tokyo, Japan), a P/Q-type Ca^{2+} channel blocker, was added to the culture medium every other day from DIV 2 (Mintz & Bean, 1993; Mikuni *et al.* 2013).

Histochemical examination

Cerebellar cultures were fixed in 4% (w/v) formaldehyde in PBS (pH 7.4) for 30 min at room temperature (RT) and incubated overnight at 4°C in PBS containing 0.3% Triton X-100, 0.12% λ-carrageenan, 1% goat serum and 0.02% sodium azide (PBS-XCG) with the following combination of primary antibodies: guinea-pig polyclonal anti-GFP antibody (1:1000 dilution, GFP-GP-Af1180-1; Frontier Institute, Hokkaido, Japan), rabbit polyclonal anti-calbindin D-28K antibody (1:2000 dilution, AB1778; Millipore, Billerica, MA, USA; calbindin is a marker protein of PCs) and mouse monoclonal anti-NeuN antibody (1:2000 dilution, MAB377; Millipore) in PBS-XCG. The samples were further incubated for 3 h at RT in PBS-XCG with the following secondary antibodies: AlexaFluor (AF) 488-conjugated goat anti-guinea-pig IgG antibody (A-11073; Invitrogen), AF 568-conjugated goat anti-rabbit IgG antibody (A-11011; Invitrogen) and AF 680-conjugated goat anti-mouse IgG antibody (A-21058; Invitrogen) in PBS-XCG. All secondary antibodies were used at a concentration of 5 μg ml^{-1}. For examination of nuclear morphology, some cerebellar cultures were stained with Hoechst 33342 (1 μg ml^{-1} in PBS; Dojindo, Kumamoto, Japan) for 15 min at RT after the secondary antibody treatment.

Immunofluorescence was observed under a confocal microscope (A1R; Nikon, Tokyo, Japan) with the following appropriate filter sets: Hoechst 33342 (excitation, 403 nm; emission, 425–475 nm), AF 488 (excitation, 488 nm; emission, 500–550 nm), AF 568 (excitation, 561 nm; emission, 570–620 nm) and AF 680 (excitation, 639 nm; emission, 662–737 nm). Images were obtained with ×10 objective or ×60 water-immersion objective lenses. The confocal pinhole size was 1.0 airy unit. In some experiments, dendrites of PCs were traced from calbindin-positive areas using Neurolucida software (MBF Bioscience, Burlington, VT, USA). The extension of dendritic trees and dendrite complexity were measured by Sholl analysis in Neuroexplorer software (MBF Bioscience; Sholl, 1953; Sawada *et al.* 2010). Concentric spheres were centred on the cell body, and the radii were incremented by 10 μm. The number of branching points within each sphere was counted, and total dendritic length was measured. The cell densities of PCs and granule cells were calculated in each culture by averaging four values of cell density measured from a single image obtained around the centre of the culture with a ×10 objective lens. These measurements were performed using NIS-Elements AR 3.2 software (Nikon).

Data are provided as the means ± SD, and n is the number of experiments. Statistical significance was tested using the Mann–Whitney U test unless otherwise stated (significance, $P < 0.05$). GraphPad Prism 5 (GraphPad Software, San Diego, CA, USA) and StatView 5 software (SAS Institute, Cary, NC, USA) were used for the analysis. In Figs 2–4 and 6–8 and Tables 1 and 2, statistical analysis was performed between cells expressing the R424H mutant and those expressing GFP alone or between cells expressing the R424H mutant and those expressing WT mKv3.3.

Expressions of heterologous proteins in *Xenopus* oocytes

The detailed procedures have been described previously (Kubo & Murata, 2001). Briefly, linearized WT or R424H mutant cDNA in pcDNA3 was used as a template to produce capped cRNA using T7 RNA polymerase (mMESSAGE mMACHINE; Ambion, Austin, TX, USA). *Xenopus* oocytes were collected from frogs anaesthetized in water containing 0.15% (w/v) tricaine. The isolated oocytes were treated with collagenase (2 mg ml^{-1}; type 1; Sigma-Aldrich) and injected with 50 nl of nuclease-free water containing 10 ng of WT *mKv3.3* cRNA, a mixture of 10 ng of WT and 10 ng of R424H mutant cRNAs, or 10 ng of R424H mutant cRNA. The oocytes were then incubated at 17°C in frog Ringer solution containing (mM): 88 NaCl, 1 KCl, 2.4 $NaHCO_3$, 0.3 $Ca(NO_3)_2$, 0.41 $CaCl_2$ and 0.82 $MgSO_4$, pH 7.6, with 0.1% (v/v) penicillin–streptomycin solution (Sigma-Aldrich) for 2–3 days before recordings.

Electrophysiological recording from *Xenopus* oocytes

Potassium currents were recorded under a two-electrode voltage clamp using an OC-725C amplifier (Warner Instruments, Hamden, CT, USA) and Clampex 10.3 software (Molecular Devices, Sunnyvale, CA, USA). The signals were digitized at 10 kHz using a Digidata 1322A (Molecular Devices). The microelectrodes were filled with an electrode solution containing 3 M potassium acetate and 10 mM KCl. The oocytes were perfused with a bath solution containing (mM): 96 NaCl, 2 KCl, 1.8 $CaCl_2$, 1 $MgCl_2$ and 5 Hepes (pH adjusted to 7.2 with NaOH). All experiments were performed at 25°C. The data were analysed using Clampfit 10.3 software (Molecular Devices) and Igor Pro 6 software (Wavemetrics, Lake Oswego, OR, USA) with the added import functionality provided by the ReadPclamp XOP of the NeuroMatic software package (http://www.neuromatic.thinkrandom.com/). To calculate conductance–voltage relationships, outward currents were activated by applying 1000 ms voltage steps from a holding potential of −80 mV to potentials up to +70 mV in 10 mV increments. The equilibrium potential of K^+ ($E_K = -104.0$ mV) was calculated from the intracellular concentration of K^+ (109.5 mM) in the *Xenopus* oocyte (Costa *et al.* 1989). To determine steady-state inactivation, cells were held at −80 mV before applying a 1000 ms prepulse to potentials between −80 and +60 mV in 10 mV increments, followed by a 250 ms test pulse to +20 mV. Steady-state inactivation (I/I_{max}) curves were fitted with the Boltzmann function, $I/I_{max} = 1/[1 + \exp(V - V_{\frac{1}{2}})/k]$, where k is a slope factor. To measure the rates of deactivation, outward currents were evoked by stepping from a holding potential of −80 mV to +50 mV for 5 ms and then stepping to potentials between −60 and +10 mV in 10 mV increments for 50 ms. The time constant of recovery (τ_{recove}) from inactivation was determined by depolarizing the cells to +50 mV for 1000 ms from a holding potential of −80 mV. A step to −80 mV of variable duration was followed with test pulses to +50 mV for 200 ms in 500 ms increments. The data points were fitted with a single exponential function. The time constants of inactivation (τ_{inacti}) and deactivation were obtained by fitting current traces with a single exponential function on the inactivating and deactivating phases of the traces, respectively.

Whole-cell patch-clamp recordings from cultured PCs

In most recordings, cerebellar cultures were constantly perfused (2 ml min^{-1}) with oxygenated artificial cerebrospinal fluid (ACSF) containing (mM): 120 NaCl, 2.5 KCl, 2 $CaCl_2$, 1 $MgCl_2$, 26 $NaHCO_3$, 1.25 NaH_2PO_4, 17 D-glucose and 0.1 picrotoxin (Tocris Bioscience, Bristol, UK; a $GABA_A$ receptor antagonist), bubbled with 5% CO_2–95% O_2 at 26°C. The other recordings were performed in Hepes-buffered ACSF containing (mM): 140 NaCl, 2.5 KCl, 2 $CaCl_2$, 1 $MgCl_2$, 10 D-glucose and 10 Hepes (pH adjusted to 7.4 with NaOH), bubbled with 100% O_2. Outward currents were recorded in Hepes-buffered ACSF containing (mM): 0.2 $CdCl_2$, 0.1 picrotoxin, 0.05 6,7-dinitroquinoxaline-2,3-dione (DNQX; Tocris Bioscience; a AMPA/kainate receptor antagonist,) and 0.001 TTX (Wako Pure Chemical Industries). Hepes buffer was used to avoid the precipitation of $CdCO_3$.

Cells were visualized on the stage of an upright microscope (BX50WI; Olympus, Tokyo, Japan) using a ×40 water-immersion objective lens with Nomarski optics and a near-infrared CCD camera (C-3077-79; Hamamatsu Photonics, Hamamatsu, Japan). Green fluorescent protein-positive cells were visualized and selected using epifluorescence optics (Olympus). Patch pipettes were made from borosilicate glass capillaries to reduce pipette capacitance (GC150F-100; Harvard Apparatus, Holliston, MA, USA) and had a resistance of 1.5–2.5 MΩ when filled with a potassium gluconate-based internal solution containing (mM): 145 potassium gluconate, 5 KCl, 0.1 EGTA, 5 Mg-ATP, 5 disodium phosphocreatine, 0.3 Na_2-GTP, 10 Hepes–KOH and 10 biocytin (Sigma-Aldrich), pH 7.3. The liquid junction potential (−10 mV) was corrected offline. Whole-cell patch-clamp recordings were conducted in GFP-positive PCs at DIV 8–10. Purkinje cells were identifiable by their large somatic size (Tabata *et al.* 2000), and their identity was confirmed by intracellular staining with biocytin. Patch-clamp recordings were acquired using a Multiclamp 700B amplifier with Clampex 10.3 software (Molecular Devices). Signals were filtered at 6–10 kHz and digitized at 10–50 kHz using a Digidata 1440A (Molecular Devices). In voltage-clamp conditions, series resistance was compensated electronically by 80–90%, and in current-clamp conditions, it was performed using the bridge balance and capacitance neutralization. Outward currents were activated with 500 ms voltage steps from −70 mV to voltages ranging from −60 to +40 mV in 10 mV increments. Leak currents were subtracted online by the *P*/4 protocol (Armstrong & Bezanilla, 1974). The recorded currents were normalized to cell capacitance, which was calculated from the transient current evoked by applying a small voltage step (−5 mV, 20 ms duration) from a holding potential of −70 mV in voltage-clamp conditions. Spontaneous excitatory post-synaptic currents (sEPSCs) were recorded at a holding potential of −80 mV for 250 s in the presence of picrotoxin and detected offline using the template search function in the Clampfit 10.3 software. Action potentials were evoked by depolarizing current pulses in current-clamp conditions (10 ms duration, from 0 to 200 pA in 10 pA increments; or 200 ms duration, from 0 to 200 pA in 20 pA increments). The resting membrane potentials were

adjusted to −60 mV by current injection. Spontaneous firing was recorded at resting membrane potential for 300 s. The half-amplitude width of the action potential was measured at the mid-point between the threshold and peak. Action potential amplitude was measured between the threshold and peak.

Fluorescence imaging of calcium

To monitor the free $[Ca^{2+}]_i$ of PCs, cerebellar cultures at DIV 8–10 were incubated with Hepes-buffered ACSF containing fura-2 AM (0.01 mM; Invitrogen) for 1 h at 37°C. The cells were visualized and perfused with Hepes-buffered ACSF at the same settings as those used for the patch-clamp recordings. For fura-2 excitation, the cultures were illuminated alternately at 340 and 380 nm wavelengths using a 100 W xenon lamp source, a fura-2 filter set (ET FURA2; Chroma Technology, Brattleboro, VT, USA), and a filter wheel (Ludl Electronic Products, Hawthorne, NY, USA). The fluorescence was filtered through a bandpass filter (470–550 nm) and captured using an EMCCD camera (iXon3 DU897; Andor Technology, Belfast, UK). The experiments were controlled by Andor iQ software (Andor Technology). The regions of interest were defined as the shape of the GFP-expressing Purkinje cell bodies. The $[Ca^{2+}]_i$ was calculated according to the previously described method with a dissociation constant of 224 nM (Grynkiewicz *et al.* 1985). The maximal and minimal fluorescence ratios (R_{max} and R_{min}) were measured after addition of the calibration solutions. The R_{max} was measured in Hepes-buffered ACSF containing 5 μM ionomycin (Sigma-Aldrich), and R_{min} in Hepes-buffered, Ca^{2+}-free ACSF containing 10 mM EGTA and 5 μM ionomycin. In some experiments, the cultures were perfused for 5 min with high-K^+ ACSF, in which 12.5 mM NaCl was replaced by equimolar KCl (total $[K^+]$, 15 mM) to elevate $[Ca^{2+}]_i$. Basal $[Ca^{2+}]_i$ was obtained as an average for a 7 min period from the beginning of the recordings, and elevated $[Ca^{2+}]_i$ for a 5 min period during high-K^+ ACSF perfusion.

Results

R424H mutant subunits exhibit a dominant-negative effect against WT mKv3.3 subunits without affecting WT subunit expression in heterologous expression systems

We examined whether the biophysical properties of hKv3.3 with the R423H mutation were conserved in mKv3.3 with the R424H mutation using the *Xenopus* oocyte expression system and two-electrode voltage-clamp recording (Figueroa *et al.* 2010; Minassian *et al.* 2012). In WT mKv3.3-expressing oocytes, depolarizing voltage steps from a holding potential of −80 mV evoked outward currents that became more apparent when the membrane was depolarized to potentials more positive than −10 mV (Supplemental Fig. S2*Aa* and S2*C*; a $V_{1/2}$ of activation of 25.5 ± 3.1 mV, $n = 19$), and the currents showed inactivation (Supplemental Fig. S2*Aa*, $n = 11$) and fast deactivation (deactivation $\tau = 0.948 \pm 0.15$ ms at −40 mV, $n = 11$; trace not shown). These results well reflected the reported properties of Kv3.3 channels, i.e. fast activation, positively shifted voltage dependence, N-type inactivation and a fast deactivation rate (Rae & Shepard, 2000; Rudy & McBain, 2001; Desai *et al.* 2008). In R424H mutant-expressing oocytes, negligible currents were observed at potentials more positive than +20 mV (Supplemental Fig. S2*Ac* and S2*B*), and the peak amplitudes were not significantly larger than those recorded in water-injected oocytes (Supplemental Fig. S2*B*; not significant by Student's unpaired *t* test), indicating that most of the currents were derived from endogenous channels present in *Xenopus* oocytes. When cRNA of WT and R424H mutant mKv3.3 was injected at a 1:1 ratio (WT+R424H), the $V_{1/2}$ of activation was significantly left-shifted, by 9.05 mV, compared with oocytes expressing WT subunits alone (Supplemental Fig. S2*C*; WT+R424H, 15.6 ± 9.2 mV, $n = 21$; WT, 24.6 ± 6.1 mV, $n = 19$; $P < 0.001$ by Student's unpaired *t* test). The value of k was decreased by 4.29 mV (WT + R424H, $k = 9.82 \pm 2.4$ mV, $n = 21$; WT, $k = 14.1 \pm 3.1$ mV, $n = 19$; $P < 0.001$ by Student's unpaired *t* test), and the time constant of activation (τ_{acti}) at +40 mV was 2.03-fold slower (Supplemental Fig. S2*Da* and S2*Db*; $P < 0.001$ by Student's unpaired *t* test). These results are consistent with previous reports of hKv3.3 with R423H mutation (Figueroa *et al.* 2010; Minassian *et al.* 2012) and indicate that the functional effects of this mutation are well conserved between humans and mice.

Coexpression of R424H mutant and WT subunits accelerates the inactivation kinetics and slows the recovery from inactivation compared with WT subunits alone

In order to reveal further the unknown biophysical properties of hKv3.3 with the R423H mutation, we investigated the inactivation kinetics, steady-state inactivation and recovery from inactivation of WT+R424H mutant channels. The τ_{inacti} of WT+R424H mutant channels was more than 2-fold faster than that of channels composed of WT subunits alone in the range of +10 to +70 mV depolarizing steps (Fig. 1*A*), and the $V_{1/2}$ of inactivation was significantly left-shifted, by 9.67 mV, compared with that of WT subunits (Fig. 1*B*; WT+R424H, $V_{1/2} = -4.39 \pm 7.09$ mV, $n = 12$; WT, $V_{1/2} = 5.28 \pm 5.33$ mV, $n = 11$; $P < 0.01$ by

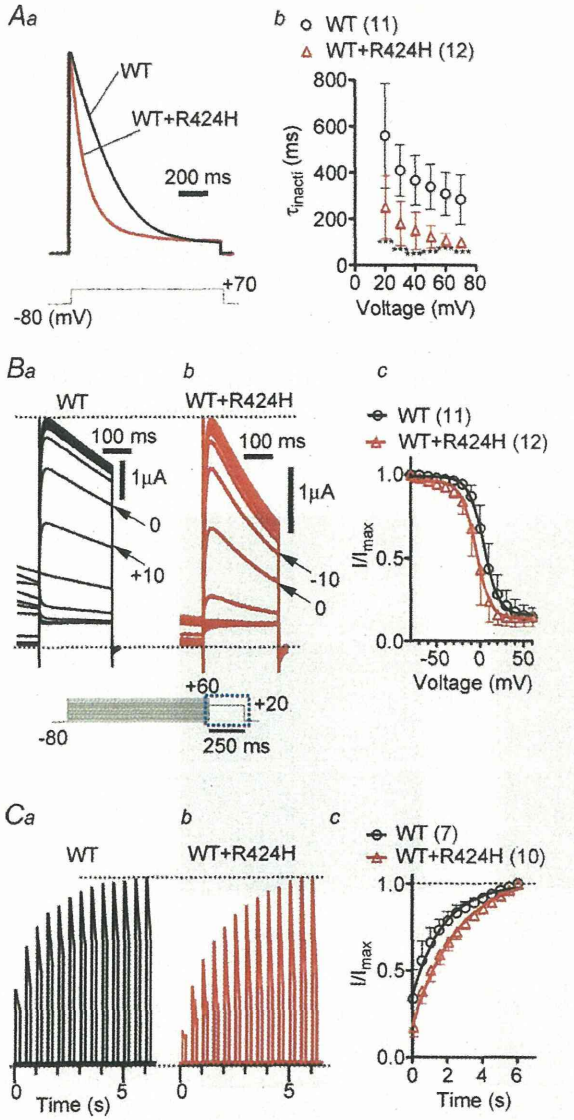

Figure 1. Coexpression of R424H mutant and wild-type (WT) subunits in *Xenopus* oocytes accelerates the inactivation kinetics and slows the recovery from inactivation compared with WT subunits alone

Aa, representative traces evoked by stepping from a −80 mV holding potential to +70 mV. The current traces are scaled to the same peak amplitude. *Ab*, the plots of the inactivation time constant (τ_{inacti}) were determined by fitting the falling phases of currents obtained in Supplemental Fig. S2*A* with a single exponential function. *Ba* and *b*, comparison of steady-state inactivation, which was obtained by changing the membrane potential from a prepulse potential ranging from −80 to +60 mV in 10 mV increments to a test voltage step of +20 mV to record tail currents. *Ba* and *b* shows traces of tail currents, and their corresponding voltage pulses are given under the traces surrounded by the dotted rectangle. *Bc*, the tail current amplitudes were normalized to the maximal current, and the resulting plots were fitted with the Boltzmann function, $I/I_{max} = 1/[1 + \exp(V - V_{1/2})/k]$, where k is a slope factor. *C*, recovery from inactivation in WT channels and WT+R424H mutant channels. *Ca* and *b*, the recovery time constant (τ_{recove}) was determined by depolarizing the cells to +50 mV for 1000 ms from a holding potential of −80 mV. A step to −80 mV of variable duration was followed with test pulses to +50 mV for 200 ms in 500 ms increments. *Cc*, time course of the recovery from inactivation. The curves were fitted with a single exponential function to obtain τ_{recove}. Here and in the following figures, error bars indicate standard deviation, the numbers in parentheses indicate the number of experiments, and statistical significance was tested using Mann-Whitney's *U* test unless otherwise stated (significance, $P < 0.05$). ***$P < 0.001$.

Student's unpaired *t* test). The τ_{recove} from inactivation of WT+R424H was significantly slower than that of WT (Fig. 1*C*; WT+R424H, $\tau_{recove} = 2.62 \pm 0.60$, $n = 10$; WT, $\tau_{recove} = 1.78 \pm 0.08$, $n = 7$; $P < 0.01$ by Student's unpaired *t* test). These results indicate that coexpression of WT and R424H mutant subunits accelerated the inactivation kinetics and slowed recovery from inactivation.

Expression of R424H mutant subunits in cerebellar cultures induces PC death and impairs dendritic development

Spinocerebellar ataxia type 13 patients show cerebellar symptoms and cerebellar atrophy, suggesting shrinkage of the cerebellar cortex and degeneration of cerebellar neurons (Waters *et al.* 2006; Figueroa *et al.* 2010, 2011). In order to explore the effects of the R424H mutant on cell survival, dendritic development and electrophysiological properties in cerebellar neurons, mouse cerebellar cultures were infected at DIV 0 with lentiviruses expressing WT or R424H mutant subunits together with GFP. Given that SCA13 is an autosomal dominant disorder and Kv3 channels are formed by the assembly of four pore-forming subunits, hKv3.3 channels in SCA13 patients are considered to be heteromultimer channels consisting of WT and mutant subunits (MacKinnon, 1991; Figueroa *et al.* 2010; Minassian *et al.* 2012). When R424H mutant subunits were lentivirally expressed in cultured PCs, the subunits were expected to incorporate into endogenous mKv3.3 channels, mimicking the pathological condition.

Green fluorescent protein fluorescence was observed after DIV 3, and >90% of PCs were GFP positive (Fig. 2*A*–*C*). In the immunohistochemical experiments, PCs were immunostained with anti-calbindin antibody and granule cells with anti-NeuN antibody. Mullen *et al.* (1992) reported that PCs are not stained with anti-NeuN antibody *in vivo*. In agreement with their report, PCs and GABAergic interneurons were NeuN negative in our culture conditions (Supplemental Fig. S3*A* and S3*B*). The mKv3.3 protein in WT-expressing PCs at DIV 10 was significantly overexpressed (by 8.3-fold) compared with that in PCs expressing GFP alone (Supplemental Fig. S3*E*). In contrast to the clear expression of mKv3.3 protein

in PCs (Goldman-Wohl *et al.* 1994), mKv3.3 expression was not detected in cultured granule cells (Supplemental Fig. S3*C*), differing from a previous report using an *in vivo* preparation (Chang *et al.* 2007). Consistent with a previous report (Tabata *et al.* 2000), the relative densities of GFP- and WT-expressing PCs decreased in a day-dependent manner (Fig. 2*A*, *B* and *D*). Until DIV 7, the relative densities of PCs did not differ significantly between R424H mutant-expressing and control cultures (Fig. 2*Aa*, *Ba*, *Ca* and *D*; $P = 0.346$ between GFP and R424H; $P = 0.222$ between WT and R424H). At DIV 11, however, the density of PCs in R424H mutant-expressing cultures was significantly decreased (Fig. 2*Ab*, *Bb*, *Cb* and *D*; $P < 0.01$ between GFP and R424H; $P < 0.01$ between WT and R424H). At DIV 14, ~40% of PCs still survived in GFP- or WT-expressing cultures (Fig. 2*Ac*, *Bc*, *Cc* and *D*), whereas there were few surviving PCs in R424H mutant-expressing cultures. Relative cell densities and the percentage of GFP-positive cells of granule cells at DIV 14 were also quantified, but there were no significant differences between R424H mutant-expressing and control cultures (Fig. 2*Ac′*, *Bc′*, *Cc′* and *E*; cell densities, $P = 0.0952$ between GFP and R424H; $P = 0.117$ between WT and R424H; and percentage of GFP-positive cells, GFP, 65.9 ± 8.3%, $n = 5$; WT, 64.0 ± 7.4%, $n = 5$; R424H, 59.8 ± 8.1%, $n = 5$; $P = 0.421$ between GFP and R424H; $P = 0.310$ between WT and R424H), indicating that expression of R424H mutant subunits did

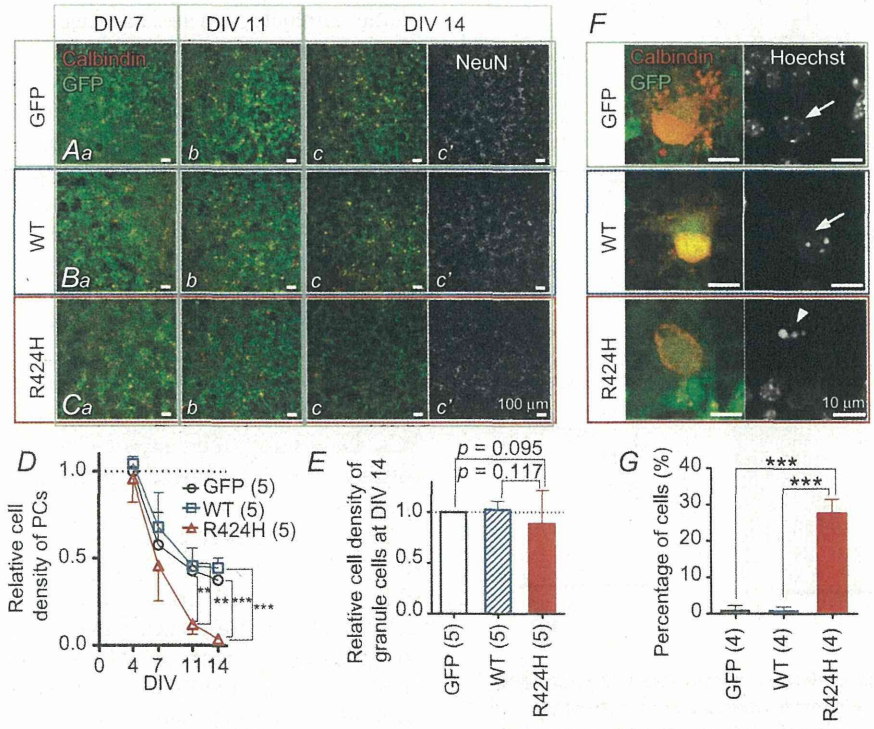

Figure 2. Lentivirus-mediated expression of R424H mutant subunits in cerebellar cultures decreases the density of Purkinje cells (PCs) but not of granule cells

A–C, immunofluorescence images of cerebellar cultures infected with lentiviral vectors expressing green fluorescent protein (GFP) alone (*Aa–c*), WT subunits and GFP (*Ba–c*) or R424H mutant subunits and GFP (*Ca–c*; see Methods). Green fluorescent protein fluorescence was enhanced by immunostaining with guinea-pig anti-GFP antibody and AlexaFluor (AF) 488-conjugated goat anti-guinea-pig antibody. Purkinje cells were visualized by immunolabelling with rabbit anti-calbindin antibody (red signals in *A–C*). *Ac′*, *Bc′* and *Cc′*, granule cells were selectively immunolabelled with mouse anti-NeuN mouse antibody (see Supplemental Fig. S3*A* and *B*). *D*, relative cell density of PCs plotted as a function of days *in vitro* (DIV). The density was normalized to the value of PCs expressing GFP alone at DIV 4. *E*, relative cell density of granule cells at DIV 14. The density was normalized to the mean cell density of granule cells in cultures lentivirally expressing GFP alone at DIV 14. *F* and *G*, R424H mutant-expressing PCs exhibiting chromatin condensation. *F*, representative fluorescence images of PCs at DIV 8. For nucleus detection, the PCs were stained with Hoechst 33342. Normal nuclei of PCs are indicated by arrows (GFP and WT), whereas a nucleus exhibiting chromatin condensation is marked with an arrowhead (R424H). *G*, summary of the percentages of PCs with chromatin condensation at DIV 8. The statistical analysis was conducted using Student's unpaired *t* tests. In the following figures and tables, the statistical analysis was conducted between cells expressing the R424H mutant and those expressing GFP or between cells expressing R424H mutant and those expressing WT subunits. $^{**}P < 0.01$ and $^{***}P < 0.001$.

not affect the survival of granule cells. The difference in cell survival between PCs and granule cells may be because cultured granule cells do not express endogenous mKv3.3 protein (Supplemental Fig. S3*C*), and R424H mutant subunits were thus unable to form multimeric channels with the endogenous mKv3.3 subunits in the cells (see Discussion). These results indicate that R424H mutant subunits induced PC death and worsened their survival in a day-dependent manner.

To examine the cell death-induced morphological defects in the nuclei of PCs, cerebellar cultures expressing GFP alone, WT mKv3.3 or the R424H mutant were stained with Hoechst 33342 at DIV 8 (Fig. 2*F*). Chromatin in nuclei of GFP- or WT-expressing PCs was stained moderately, with some small bright granules (Fig. 2*F*, arrows in GFP and WT panels), demonstrating normal nuclear morphology. In contrast, PCs expressing R424H mutant subunits showed clear chromatin condensation (Fig. 2*F*, arrowhead in R424H panel). The percentages of PCs exhibiting this chromatin condensation were significantly different between R424H mutant-expressing PCs and the control group (Fig. 2*G*; $P < 0.001$ by Student's unpaired t test). These results suggest that the expression of R424H mutant subunits might induce apoptotic cell death in PCs.

At DIV 7, several neurites were observed in GFP- and WT-expressing PCs, which had morphologies similar to those of R424H mutant-expressing PCs at this stage (Fig. 3*Aa′*, *Ba′* and *Ca′*). However, at DIV 11, GFP- and WT-expressing PCs had elongated immature dendrites, whereas R424H mutant-expressing PCs did not show dendritic extension (Fig. 3*Ab′*, *Bb′* and *Cb′*). Sholl analyses of the dendritic arbors revealed that the number of dendritic intersections in R424H mutant-expressing PCs was significantly smaller than that in GFP-expressing (Fig. 3*D*, at distances of 10–50 μm from the cell body; $P < 0.01$) or WT-expressing PCs (Fig. 3*D*, at distances of 10–40 μm; $P < 0.01$). These results clearly demonstrate that in addition to the induction of cell death, expression of R424H mutant subunits in PCs decreases the survival rate and impairs dendritic development.

R424H mutant-expressing PCs exhibit lower outward current density

The results using *Xenopus* oocytes showed that expression of R424H mutant subunits significantly modulated WT mKv3.3 channel function (Fig. 1 and Supplemental Fig. S2). Thus, similar effects would be predicted in PCs lentivirally expressing R424H mutant subunits. In order to determine how these electrophysiological properties were affected, whole-cell patch-clamp recordings were performed using cultured PCs expressing GFP only, WT subunits or R424H mutant subunits at DIV 8–10.

Purkinje cells could be identified by their large cell bodies (cell body diameters of PCs at DIV 10, 17.2 ± 2.6 μm, $n = 78$; those of other neurons, 7.26 ± 1.7 μm, $n = 226$), and the recordings were confirmed by a combination of intracellular staining and immunocytochemical staining (Supplemental Fig. S4*A*). The cell capacitance of R424H mutant-expressing PCs was significantly lower than that of GFP- or WT-expressing PCs (Table 1; $P < 0.001$ in R424H *versus* GFP and in R424H *versus* WT), reflecting the impairment of dendritic development (Fig. 3*D*). However, the resting membrane potential and input resistance of R424H mutant-expressing PCs showed no difference when

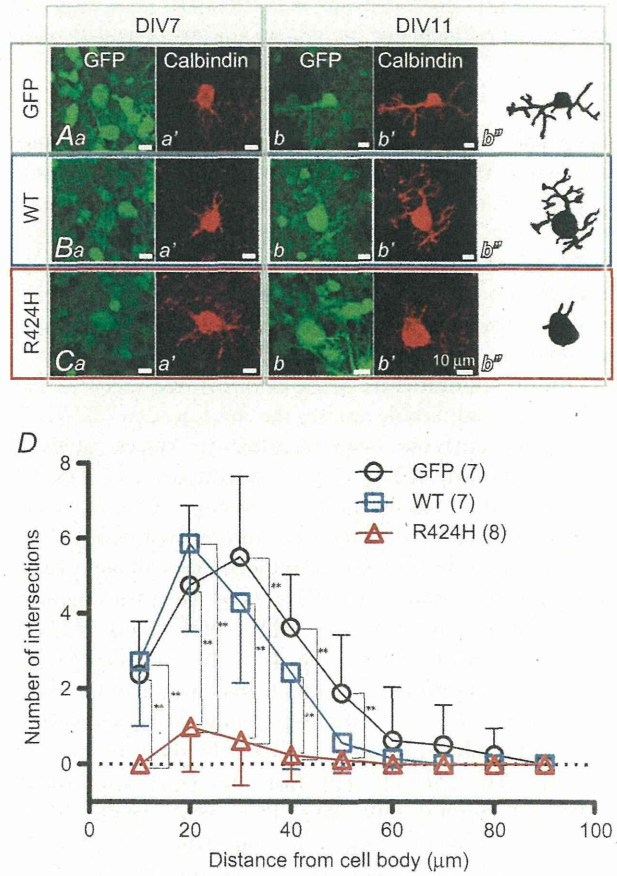

Figure 3. R424H mutant-expressing PCs exhibit impaired dendritic development
A–C, immunofluorescence images of PCs expressing GFP alone (*Aa–b′*), WT subunits and GFP (*Ba–b′*) and R424H mutant subunits and GFP (*Ca–b′*). *Ab″*, *Bb″* and *Cb″*, morphology of PCs expressing GFP (*Ab″*), WT subunits and GFP (*Bb″*) and R424H mutant subunits and GFP (*Cb″*) are depicted for clarity. Each PC was traced using Neurolucida software. *D*, summary of dendrite complexity measured by Sholl analysis. Concentric spheres were centred on the cell body, and the radii were incremented by 10 μm. The number of branching points within each sphere was plotted as dendrite complexity (i.e. the number of intersections). $^{**}P < 0.01$.